

Plasma dynamics in PF-1000 device under full-scale energy storage: I. Pinch dynamics, shock-wave diffraction, and inertial electrode

V A Gribkov^{1,2,3}, B Bienkowska¹, M Borowiecki¹, A V Dubrovsky²,
I Ivanova-Stanik¹, L Karpinski¹, R A Miklaszewski¹, M Paduch¹,
M Scholz¹ and K Tomaszewski¹

¹ Institute of Plasma Physics and Laser Microfusion, ul. Hery 23, Warsaw 01-497, Poland

² Institute for Theoretical and Experimental Physics, B Chermushkinskaya ul. 25, 117218 Moscow, Russia

³ Abdus Salam International Centre for Theoretical Physics, Strada Costiera 11, 34014 Trieste, Italy

E-mail: gribkovv@yahoo.com

Received 28 June 2006, in final form 11 December 2006

Published 16 March 2007

Online at stacks.iop.org/JPhysD/40/1977

Abstract

This paper (paper I) presents the first part of results obtained with the PF-1000 facility for the first time at its upper energy limit (≈ 1 MJ). Special attention is paid here to plasma ('pinch') dynamics, which was investigated in relation to its electro-technical and radiation (especially neutron) characteristics with the help of a number of diagnostics, both time-integrated and with nanosecond temporal resolution. In these methods we utilized a Rogowski coil for the routine electro-technical measurements, visual multi-frame and streak cameras, soft x-ray pin-hole multi-frame cameras, PIN-diode assembly and PM tubes with scintillators for soft and hard x-rays as well as for neutron investigations together with a set of activation counters. In particular, the temporal cross correlation of different phenomena taking place during the discharge was investigated. The pinch's longevity appears to be 10–15 times larger than the ideal magnetohydrodynamic growth time (ratio of the pinch radius to the ion thermal velocity). It is demonstrated how the 'target' dynamics (pinch plasma of the dense plasma focus (DPF)) depends on and may be controlled by the electrode's size and the geometry of the chamber in this large-scale device. Diffraction of a shock wave together with a current sheath on an obstacle made at the DPF anode cap opens an opportunity for an inertial electrode to be used in future at larger DPF devices.

1. Introduction

Dense plasma-focus (DPF) [1] is a gas-discharge installation with two cylinder metallic coaxial electrodes. It belongs to the Z-pinch class and operates with a cylindrical insulator positioned at the lower part of the internal electrode (anode). Initial pressure of the working gas is equal to a few torr. Temporal evolution of the discharge undergoes as a rule the following several phases.

The first stage is gas breakdown developing along the exterior of a cylindrical insulator. This surface discharge

[2] takes from a few to a hundred nanoseconds and bears non-equilibrium kinetic (K) character (acceleration of initial charged particles, streamers, avalanche, etc [3]).

The second stage is of a magnetohydrodynamic (MHD) nature. It is an inverse pinch, when the plasma sheath expands from the insulator to the cathode bars, being stable all the time.

The third stage, being relatively long (several microseconds for medium- and large-scale facilities), is also mainly of an MHD nature [4]. It starts after the second stage with supersonic plasma acceleration by an azimuth magnetic field

of the discharge current and matures with the implosion of the plasma onto the Z -axis of the chamber. There are two types of electrode systems of DPF—the Filippov configuration, where plasma accelerates to the chamber's Z -axis radially along the flat anode immediately after the second stage, and the Mather one where plasma accelerates first next to the anode tube elongated up to Z -axis and only after this stage does it turn around the edge of the tube and implode radially. The speeding up plasma (plasma-current sheath (PCS)) is contained during its movement to the chamber's axis between a shock wave (SW) in front of it and a current sheath (CS) behind the SW. The discharge current at this time is subdivided inside the DPF chamber into four non-equal parts [5–7]:

- (1) Current flowing along the front of the SW.
- (2) Skin-layer current at the backside of the PCS (constituting the main part of the current, which is established in this device during the so-called 'working regime of DPF operation' after passing through a set of conditioning shots); it pushes the PCS to the chamber axis.
- (3) Residual current flowing behind the PCS throughout low-density plasma, which has been incompletely captured by the PCS; this current produces turbulence in the residual plasma and produces the 'third type of insulation'—isolation of the main part of current flowing within the PCS and later on through a *pinch* (dense plasma column) from the surrounding residual plasma.
- (4) Remanent current on the insulator surface (which is not present in some DPF devices).

However this phase also bears evidence of some kinetic phenomena [6, 7], namely micro-turbulence within the skin-layer of PCS, making the sheath more rigid in relation to the flute instability from the side of short wavelengths, runaway electrons accelerated both at the front of the converging quasi-cylindrical shock wave and within the PCS and turbulence of residual plasma.

This stage is completed first by a convergence of the SW on the Z -axis (singularity line for the azimuth magnetic field) accompanied (in the case when deuterium is used as a working gas) by runaway of its part of the current. These fast runaway electrons ('runaways') form a thin filament near the Z -axis (of a diameter equal to circa the SW front) and produce medium-energy x-rays (with energy of photons about 30–50 keV) (see e.g. [6, 8]). Then, some tens of ns later, this phase finishes by the maximum plasma compression on the chamber axis Z , with confinement of this *pinch* plasma for circa 100 ns. This phase is accompanied with plasma cooling due to radiant and electron conductivity. Soft x-ray (SXR) radiation (of about 1 keV photon energy) is produced during this process. It is clear that during this period, known in the literature as the so-called 'first compression' stage, three 'pinches' in fact exist [8]:

- (1) 'current pinch' occupying the biggest diameter (~ 10 cm) and including in itself almost total discharge current (seen by magnetic probes and due to Faraday rotation measurements);
- (2) 'dense plasma pinch' (~ 1 cm) containing dense plasma imploded about the chamber axis (seen by interferometry) and carrying circa 70% of the discharge current; and

- (3) 'bright plasma pinch' (a few mm of diameter), which is positioned about the Z -axis and usually related to current/plasma filamentation (runaways) taking place near this line of the magnetic field singularity and seen by soft x-ray pin-hole camera.

The main aim of the present paper is to describe a specificity of *plasma dynamics* under full-scale energy storage of the PF-1000 facility.

The next stage is a short-lasting event of kinetic (K) character (a few tens/hundreds nanoseconds) [6–10], which will be discussed in detail in paper II. It starts from the so-called 'current abruption' phenomenon when the pinch is disturbed by the Rayleigh–Taylor instability provoking in turn various micro-instabilities. These non-linearly coupled instabilities, practically instant (during a time period much shorter than 1 ns), substitute the classical collisional current within the pinch by the collisionless stream of fast electrons having characteristic energy of several hundred keV. The latter *fast electron beam* generates hard x-ray radiation on the anode [4, 7, 8, 11, 12]. Then these fast electrons are magnetized and the whole current is carried mainly by fast ions [13] having a spectrum extended to several MeV.

The first MHD phase forms a 'target'—hot (≤ 1 keV) compressed ($\leq 10^{19}$ cm $^{-3}$) plasma, whereas during the second one (K) the powerful beams of fast electrons and ions are generated and start to interact with plasma and electrodes. A noticeable part of the fast ion stream composed of 'medium' energy particles (usually in the range 50–150 keV) is captured by a magnetic field of the pinch and confined within the plasma 'target' for a period of about 10 drift times [14]. Interactions of these ions—both Coulomb and direct fusion ones—with the above-mentioned plasma target (at the operation of DPF with deuterium or deuterium–tritium—(DT)—mixture as a working gas) result in neutron emission [14, 15]. Energy E_c , released from capacitors to the discharge, is in the range from just a few joules to circa 1 megajoule (MJ).

At the present time there is a rapidly increasing field which includes various applications of *small-* and *medium-size* DPF installations. The new high-current technology [16] introduced in these devices provides an opportunity for reliable exploitation with a high repetition rate (up to tens of cps) and ensures its long lifetime (circa 10^7 discharges) [17]. According to our experience at least three modern elements have to be introduced in any new DPF device of small or large scale: capacitors of the assembly similar to KMK type, pseudo-sparks as main switches and DPF chambers manufactured by means of e-beam or laser welding having no rubber o-rings [16, 17]. Such a device may be used as a source of radiation for various types of goals of the semiconductor industry (projection and proximity x-ray lithography, micromachining), biology and medicine, in material sciences, etc [17–21], and it will have a reliable operation during a million-shot run with a repetition rate of tens of cps (if the proper cooling can be organized).

As to the fame of the *big* DPF facilities, it is based on the fact that the large-scale DPF might be a very intense and efficient neutron-producing device. The scaling law for the neutron yield has been formulated at the beginning of the plasma focus investigations: $Y_n \approx E_c^2$, where Y_n is the DPF absolute neutron yield per shot and E_c is its bank energy. It

is very promising for the efficiency of neutron production, namely for large facilities having a high value of E_c . However, later on the investigations carried out with the biggest devices of that time revealed that a certain limit existed for bank energy, above which the scaling law with those installations was not fulfilled [22]. Apart from the failure of fusion perspectives, even now this experimental fact is a serious preclusion for a particular use of a big DPF. We mean its possible exploitation as a powerful source of *fusion* neutrons for material sciences, namely as the source for testing of materials perspective for the first wall components and construction elements in magnetic confinement fusion and, especially, in inertial confinement fusion reactors (where the neutron interaction with materials will be of the ‘explosive-like’ type—the same as within a DPF).

Indeed, the present-day expectations in this field related to the IFMIF facility [23] are based on a powerful high energy deuteron accelerator (about 40 MeV, 0.5 A). It is thought that it will be able to ensure, during a one-year irradiation term, neutron fluence on the levels from 0.01 upto 50 displacements per atom (dpa) in various zones positioned near a target having area $5 \times 20 \text{ cm}^2$. The value of 1 dpa corresponds to the irradiation, e.g. of iron-based specimens (counted as the prospective ones for a fusion reactor [24]) with the *mean* neutron flux $4.5 \times 10^{16} \text{ n m}^{-2} \text{ s}^{-1}$ during a year. One dpa is approximately equal to a total fluence of 10^{21} neutrons per cm^2 for Be- and C-based materials. The total cost of the IFMIF is estimated to be above the level of 10^9 US\$ with the operating cost of circa 6×10^7 US\$ per year. Projected construction time of this notable facility is about 10 years.

However the above new run-up operational DPF technology might be fit for the construction of an effective 0.5–1.0 MJ DPF facility (thus on the level of present-day devices) working on DT mixture with a current of the order of 5.5–6 MA and in a high repetition mode. The cylindrical shape of the plasma neutron source in this device will be characterized by a diameter of 1 cm with a length of 10 cm. In this case such a device could ensure, during a one-year run, an overall fluence of the order of 0.1–1.0 dpa with its total and operational costs two orders of magnitude less compared with the abovementioned. What is more, this kind of facility can be constructed and put into operation in a three-year period. Thus this device might easily fill the niche between *fission* reactors (having no proper neutron spectrum), used at the moment for the above purpose, and IFMIF. But to reach this aim the neutron yield of the DPF of a few hundred kJ must follow the above scaling law $Y_n = 10^{10} I_p^4$ for deuterium as a working gas (where I_p is the current *flowing through the pinch*, measured in MA).

It means that if in the facility of PF-1000 type [25] the pinch current were about 6 MA its neutron yield will exceed 10^{13} of 2.5 MeV neutrons/pulse. It will give $>10^{15}$ for the 14 MeV neutrons at the operation of the DPF with the deuterium–tritium mixture as a working gas. Taking into consideration the possible geometry of the near-pinch anode part of the DPF of this energy level, it is easy to estimate that 1 dpa can be achieved during an operational year in a volume of about 1 litre with the irradiation area $\sim 0.1 \text{ m}^2$. For all that, a PF must work with a repetition rate of 3–4 cps with

the irradiating zone positioned 0.1 m apart from specimens. During a one-year run the main parts of the device (capacitors and switches) will be changed 10–20 times. These figures for a facility, designed with the use of the abovementioned new technology, look feasible since for several years we already have DPF devices working with a repetition rate 3–16 cps [17] whereas with our recent PF-6 device [26] we reached a current circa 760 kA and neutron yield Y_n about 10^9 neutrons per pulse with deuterium as a working gas with four capacitors having the overall energy bank $E_c = 7 \text{ kJ}$ only. According to our experience in scaling law for bank parameters the above-mentioned figures might be expected for the same type of DPF-based neutron test facility at the level of a few hundred kJ.

As for the abovementioned saturation of the DPF neutron yield, several phenomena responsible for the effect were found during the last two decades. We shall discuss their physics elsewhere, but here we would just like to mention that in our point of view it is possible to get over these difficulties, and here we shall analyse some of them, which are intrinsic to the PF-1000 device.

But there is something more in this sphere. This project in the field of radiation physics and chemistry of material science (in the case of success in the above scaling) could be aimed to develop a new field within the area. Namely, it might ensure radiation tests at *heightened* conditions thus *shortening* the test periods of candidate radiation resistive materials (e.g. beryllium, tungsten, ceramic composites, austenitic and ferritic steels, lithium, etc) being designed to meet the needs of fission and fusion power engineering, space industry and accelerator technology.

In fact, in the field of radiation tests of materials there is a unique opportunity to shorten the period of testing sessions. Indeed such a device enables us to ensure a *peak* power flux density of neutron radiation in the range $10^{23} \text{ n cm}^{-2} \text{ s}^{-1}$ (or its energy density up to $10^{10} \text{ J cm}^{-3}$). It is even higher for *e-* and *i-* beams as well as for plasma streams generated by DPF. Thus it seems to be tempting in such experiments to produce, just during a few shots, the same effects as under exploitation of classical radiation devices *for years* when operated at the much lower working power flux density. What is more, many major problems can be investigated here—atom displacements, blistering, erosion, redeposition and material migration, fuel recycling and retention, etc possibly during a very short period of time. It seems that it would also generate material-specific activation and radiological property data and support the analysis of materials for use in safety, maintenance, recycling, decommissioning and waste disposal operations.

Thus potentially it can give an opportunity to sustain a rate of material investigation and their selection (e.g. for space vehicles and fusion devices like ITER, NIF or Z-machine) in a proper time regime in relation to fusion program development. But of course for this aim a so-called ‘*damage factor*’ should be established, i.e. a dependence of both damage degree and its nature (side by side with other interaction effects) on power flux density, i.e. on energy and pulse duration of penetrating radiation. Dependence of the damage factor on elemental contents of materials should also be investigated as well.

However another point becomes an issue for such a big, powerful device, having high repetition rate. Namely, simple

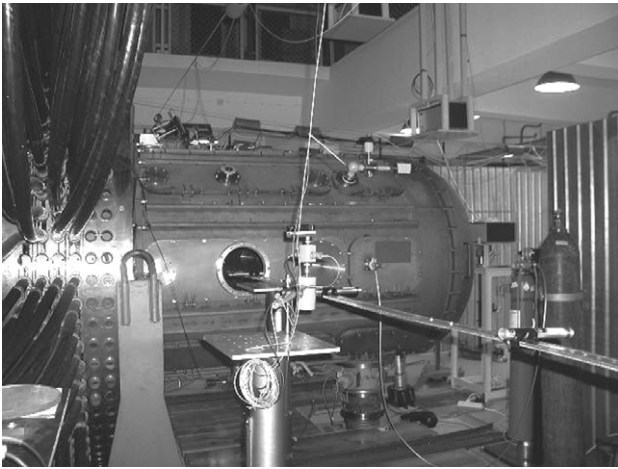


Figure 1. The PF-1000 facility.

estimations show that in the above DPF facility working as a repetitively pulsed neutron source an average heat power released onto the metallic surface in the centre of its anode could reach circa 1 MW cm^{-2} . It implies serious (if resolved at all) problems for the material of the central anode's part of a DPF chamber.

We shall present in this paper our recent results taken from the investigation of the operation of the PF-1000 facility, which exploits deuterium as a working gas in a single-shot mode on the energy level close to the maximal one between all other devices of this type (0.6–1.0 MJ). We intend to discuss these data in view of the abovementioned problems and possible means for solving them.

2. The apparatus

The PF-1000 facility [25], manufactured on the basis of the corresponding technology of the 1970s, has nevertheless the largest bank operating on the energy level of about 1 MJ, and it operates with deuterium as a working gas (figure 1).

It consists of the following main units:

- vacuum and gas assembly which includes vacuum chamber (right-hand side of figure 1) with coaxial electrodes and vacuum/gas handling systems,
- condenser bank positioned on two other levels of the building ($E_c \cong 1.056 \text{ MJ}$ at initial charging voltage up to $U_0 = 40 \text{ kV}$) and pulsed electrical power circuit with high-pressure spark-gaps, low-inductance coaxial cables, a collector (left-hand side of figure 1) and a control room.

After engaging the spark-gaps, energy, which has been stored in the bank, is transferred by means of coaxial cables through the collector to the electrodes of the DPF chamber. The vacuum chamber which contains the electrodes has a large volume (1400 mm in diameter and 2500 mm in length).

Two families of electrode geometries differing essentially in their inter-electrode gaps, lengths and shape were used in this set of experiments. The copper *anode* has a diameter of 230 mm with a length of 600 mm. This anode had on the top of it a cap, which in two dissimilar types of experiments had a diameter equal to or slightly larger than the anode tube itself (figure 2(a)). In the second case the protrusion of the cap

outside the anode tube was manufactured as a circular hat-shaped 'tooth' on its end (in fact the anode cap was of radius 1 cm larger than the anode cylinder itself). Its primary aim was to grasp excessive metallic debris possibly produced and entrained by the current sheath from the anode on its way to the Z-axis of the DPF chamber. But it constitutes a small obstacle for a shock wave (SW) pushed by a magnetic field of a current sheath (CS). This SW stumbles on the obstacle when arriving at the edge of the anode.

Figure 2(b) is an example of the first type of *cathode* electrode system. It is made as a squirrel cage which consists of 12 stainless-steel rods each of 40 mm diameter and 800 mm length, distributed around a 400 mm diameter circumference. In figure 2(c) we show a second type of squirrel cage cathode—24 stainless steel rods 32 mm in diameter and with a length of 600 mm. They were also distributed around a 400 mm diameter perimeter with the same anode and insulator. As may be seen in figure 2(a) (left side) and (b) the cathode rods in the first case are much longer than the anode. In the second configuration (figure 2(a)—right side, (c)) some of them are equal to the anode's length with the others being slightly longer (by a value of less than half the pinch's length). The cylindrical alumina insulator sits on the lower part of the anode. The main part of the insulator extends 113 mm along the anode into the vacuum chamber. The condenser bank of capacitance $1320 \mu\text{F}$ (264 capacitors having $5 \mu\text{F}$ capacitance and 40 nH inductance each) was charged in these experiments to the voltage U_0 varying between 20 and 40 kV, which corresponded to discharge energies E_c ranging from 264 to 1056 kJ. Usually the bank was exploited on the level of 810 kJ and 35 kV, respectively.

In this set of experiments with PF-1000 compared with previous research [27–30] the energy increase was due to the bank *capacitance* increase (*not* a voltage rise as was the case previously with these devices). And, as circuit/chamber matching demands, the electrode dimensions were increased in relation to the previous ones in an attempt at harmonizing external and internal inductances of the gun and equalizing the current quarter of the period with the plasma collapse time. This device operates at a rate not higher than 1 'shot' per 10 min.

3. Experimental arrangement

The overall scheme of the experimental set-up is shown in figure 3. To study the MHD evolution of plasma, a three/quarter frame optical camera with exposure time of about 1 ns was employed (see figure 4). The delay between the subsequent frames is in the range 10–20 ns. An interference filter ($\lambda_{\text{max}} = 593 \text{ nm}$, FWHM = 6 nm) recording only continuum radiation far from spectral lines was put into the optical path of the passive optical diagnostic subsystem. In addition to this diagnostics a visible streak camera was also used. In this camera its slit was positioned perpendicular to the Z-axis of the chamber. It ensures measurements of the radial plasma CS and SW speeds and gives information on the implosion symmetry.

Two types of the four-frame SXR cameras have been applied in order to obtain plasma images in the soft x-ray range—one based on an open microchannel plate (MCP)

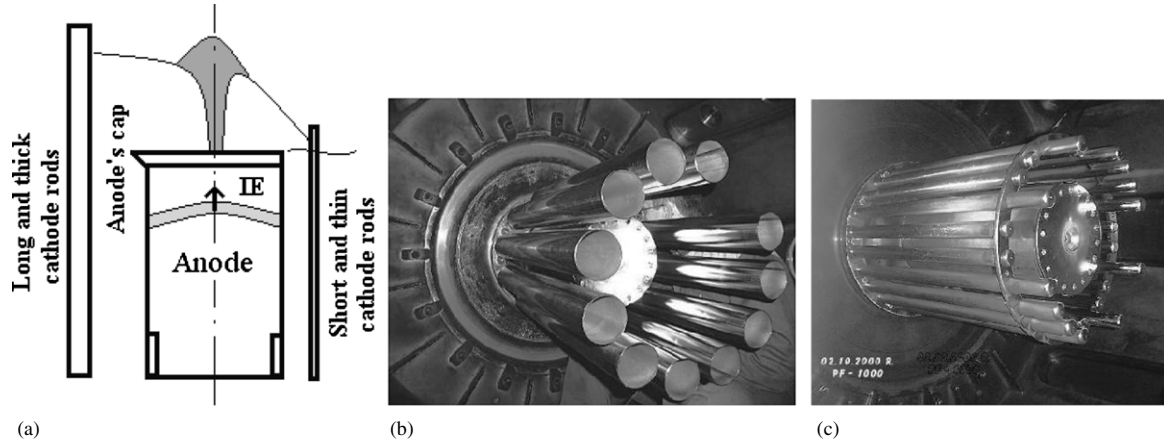


Figure 2. Electrodes set-up: (a)—scheme of two variants—left and right—of cathode rods and a cap of the anode and their pictures—(b) and (c).

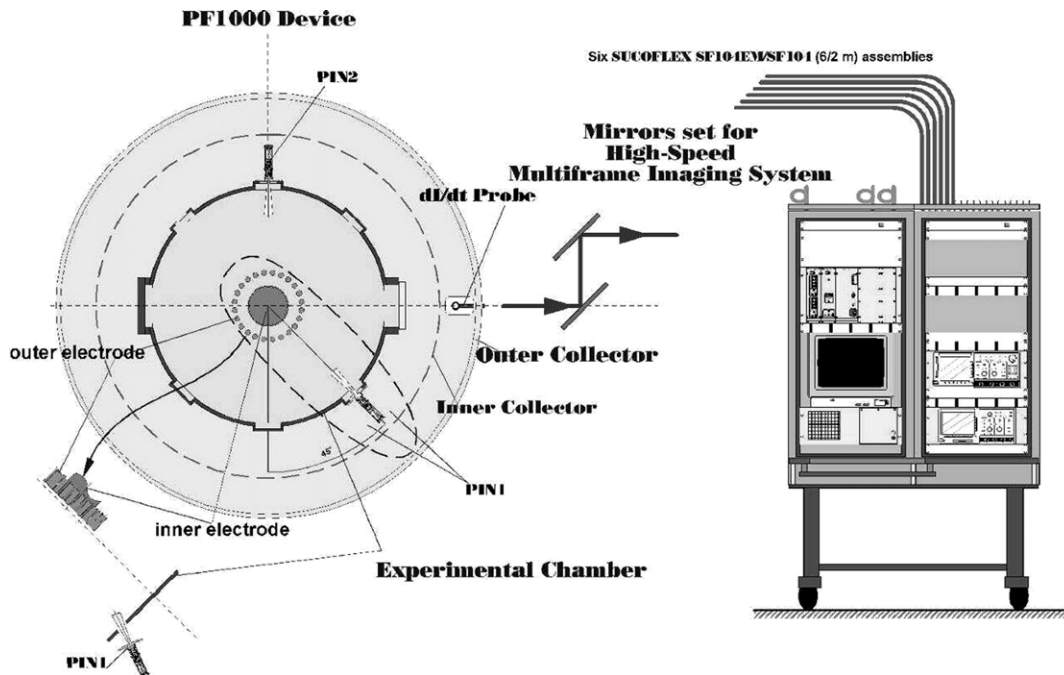


Figure 3. Scheme of the experimental set-up.

device (figure 5) and another just a time-integrated pin-hole camera with a x-ray film registration. Regardless of construction details the first camera has an MCP and phosphor screen, divided into four electrically independent sectors. The screen is attached to a fibre optics plane-plate separating the vacuum inside the camera from the atmospheric pressure outside. Each sector is gated by a single (positive) electrical pulse with an amplitude of 5–6 kV applied between a phosphor screen and the input side of MCP, which is connected to a common ground. Its activation is produced for a time interval 1 ns with a delay of 10–20 ns with regard to others.

The MCP is charged automatically through a capacitor divider formed by a gap between the MCP and MCP-screen. After applying a voltage pulse to any sector, SXR radiation is converted into an electron flow, which is amplified inside the MCP and converted by a phosphor screen into visible light

outgoing from a fibre optic plate. Both SXR cameras were used *side-on* to Z-axis.

Time-resolved measurements of soft x-ray (SXR) radiation were also made by means of PIN diodes covered with different filters. One of these signals from a PIN diode was used for synchronization purposes and for the determination of the temporal relation between the SXR radiation of the plasma and the frame images recorded by means of optical and x-ray diagnostics.

We investigated the neutron production process by measuring its time evolution, the anisotropy and the absolute neutron yield on the basis of both time-integrated methods and time-resolved registration of neutron pulses at different angles to the electrode axis, as well as by their comparison with time-resolved and time-integrated measurements of the soft, hard x-ray radiation and the fast electron and ion beams.

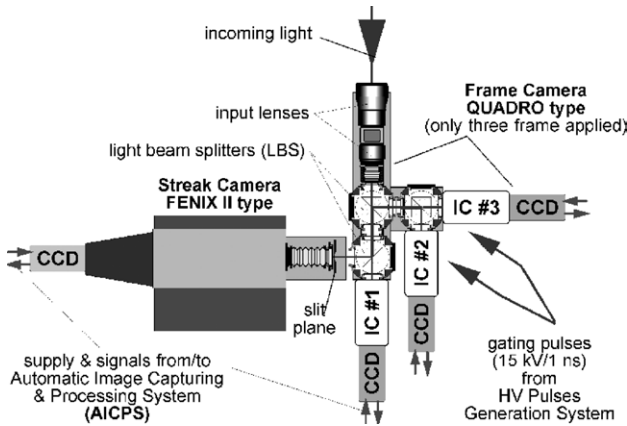


Figure 4. General layout of the passive optical diagnostics subsystem.

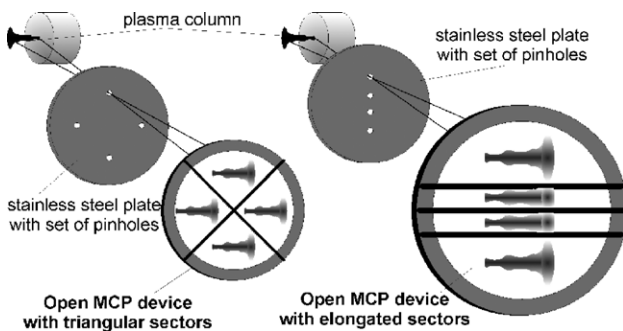


Figure 5. Schematic diagram of the set-up of the four-frame SXR camera.

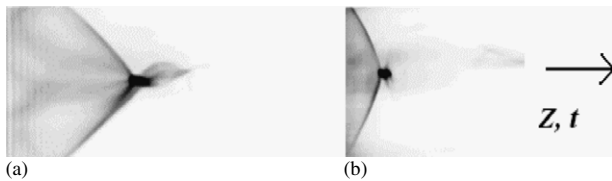


Figure 6. Streak-camera pictures made for shots with low (a) and high (b) neutron yield (first shot belongs to ‘conditioning’ shots whereas the second one reflects a ‘working’ regime).

The total neutron yield (Y_{tot}), i.e. the number of neutrons produced during a single discharge (‘shot’) and emitted in various directions, was measured taking into consideration the data received by means of five silver-activation counters (SC) placed at equal distances and different angles around the PF-1000 experimental chamber.

Three scintillation-photomultiplier detectors (SPD), located at different angles—head-on (0° , SPD1), side-on (90° , not shown in figure 6) and back-on (180° , SPD2)—all of them 7 m distant from the electrode outlet, were used to perform time-resolved measurements of the hard x-ray radiation and neutron emission, pulses of which were separated on the oscilloscope traces due to the corresponding time of flight. An investigation of electron and ion beams generated in the facility was done by a number of diagnostics using Cerenkov detectors and special track detectors. These means of fast particle investigation, as well as results received from them, are described in the following paper II. Special electrical and optical synchronization arrangements allowed the synchronizing

of all diagnostics with the PF phenomenon with a temporal precision of 5 ns.

4. Experimental results and discussions

The first series of observations was carried out at the PF-1000 facility in the operational regime with a deuterium pressure range $\cong 2\text{--}4$ Torr and with a discharge energy level up to 850 kJ. In these series the chamber had long cathode rods as shown in figures 2(a) (left) and 2(b) and the anode’s cylinder was smooth and even with its flush-mounted head. In these conditions the discharge current was 2.5–3 MA. Neutron emission Y_n was of the order of $5 \times 10^{10}\text{--}2 \times 10^{11}$ n/shot with the maximum neutron yield of 6×10^{11} measured by five silver and three indium activation counters taking into consideration the neutron yield anisotropy. Each shot with the highest neutron yield was preceded by two so-called ‘conditioning’ discharges, obtained with a lower charging voltage and a relatively higher initial pressure of gas. Such a procedure noticeably increases reproducibility of all ‘working’ shots and the absolute value of the best ones. The results obtained during these series in relation to the pinched plasma can be summarized as follows:

- (1) It was found that for each initial filling pressure value (p_0) the neutron yield (Y_n) increases as a function of the charging voltage (U_0) up to a certain maximum and after that it decreases in spite of a further increase in U_0 .
- (2) The same behaviour of neutron yield was found for the situation when for a given charging voltage U_0 we increased the initial deuterium pressure—after a certain maximum it decreases in spite of a further increase of p_0 .
- (3) Charging voltage increase produced *in parallel* with the initial pressure rise (provided that for *each initial pressure* we used the above *optimal* charging voltage) resulted in a further increase in neutron yield. No saturation in neutron yield was found up to 35 kV.
- (4) Two neutron pulses were observed in most of the discharges, as is usual for these devices having about the same pulse duration and interval between the two peaks (≈ 150 ns FWHM for all of them), and typically in our case the second pulse was four to six times larger in amplitude than the first one (see however discussion on this point about the impact of scattered neutrons in the following paper).

Our investigations of the current sheath (CS) collapse dynamics performed by means of a streak camera for the shots with low and high neutron yield are presented in figures 6(a) and (b), respectively. One may see very different implosion velocities of CS and the degree of their symmetry. Both are much better in the case of high neutron yield (figure 6(b)). In good shots for the speed v_{im} we have received usually a value equal to $2\text{--}5 \times 10^7$ cm s $^{-1}$.

Five typical sequences, consisting of three-frame pictures, each taken during one shot in the visual wavelength range, are put together in figure 7 in a single set according to the time synchronization. These sequences were selected for the operation of the device *in the same conditions* and *with similar neutron yield*. From this figure we determine the CS speed also on the level $\geq 2\text{--}5 \times 10^7$ cm s $^{-1}$ changing from shot to shot. One may observe a collapsing process of the CS preceded by a

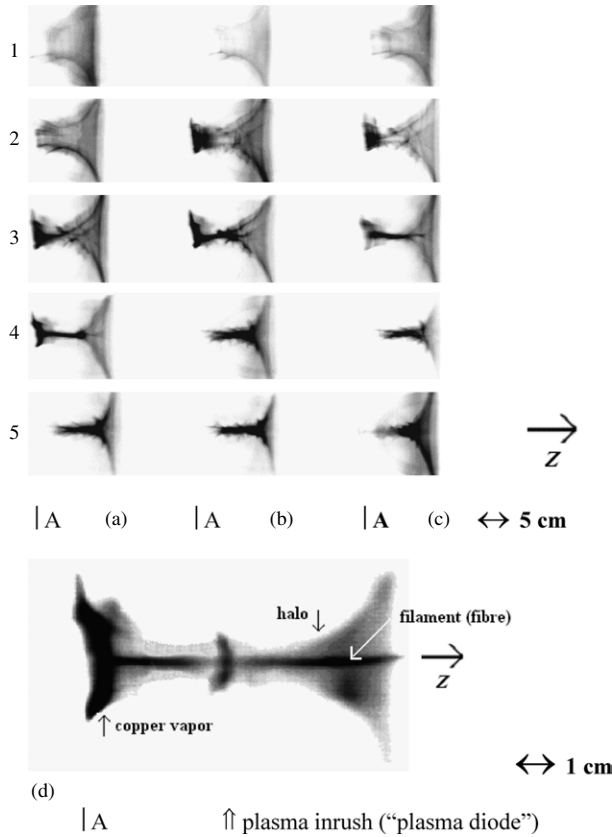


Figure 7. Set of visible frame camera pictures of pinching dynamics (time sequence develops from left to right: (a), (b), (c) and from the top to the bottom of the picture 1 to 5 with ‘A’—anode position) and (d)—an enlarged example of the pinch with ‘filament’, ‘halo’, ‘plasma diode’ and copper vapours at the anode surface.

SW (double structure of the converging plasma shell—images 1 and 2(a), (b), (c) plus 3(a) of figure 7), then the formation of a straight and bright column (filament) with a ‘halo’ of lower luminosity (3(b) through 5(b) and an enlarged picture (d) in the same figure) all having a height of its cylindrical part approximately 8–10 cm. The average diameter of the filament during the period of its luminescence is less than 0.2 cm whereas the ‘halo’ is 0.9 cm diameter (see a separate picture 7(d) and also figure 8). Maximal plasma compression precedes the current dip by ≈ 100 ns and takes place about $2 \mu\text{s}$ after the current maximum.

Implosion speed measured by the above three methods gives us a lower estimate of the plasma temperature T in the dense plasma pinch provided that the ordered kinetic energy of the PCS is converted into chaotic plasma particle motion: $(m_d v_{\text{im}}^2)/2 = 3/2(kT)$ and that additional plasma heating takes place because of the final adiabatic plasma squeezing (see [4, 8] and references therein). It appears to be in the range from $T \cong 0.5$ to 2.5 keV. Let us take $T \cong 0.9$ keV as an average for the most typical implosion velocity $3.5 \times 10^7 \text{ cm s}^{-1}$ and eventually $T = 1.3$ keV taking into consideration the ultimate adiabatic compression. Then taking into consideration Bennett’s equation $H^2/8\pi = 2nkT$ (where H is magnetic field about the pinch border) and supposing that the whole current measured flows through the pinch, the density will be circa $2 \times 10^{19} \text{ cm}^{-3}$. If we take into

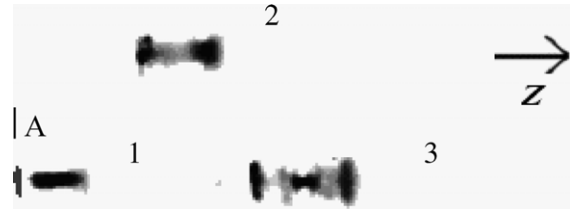


Figure 8. Three-frame time-resolved x-ray pictures obtained for the case of long cathode rods (1, 2 and 3: frames in the clockwise direction as shown by digits) with anode positions (A) seen as vertical dark lines on the left-hand side of each image.

account a current decrease to the moment of maximal plasma compression and suppose that only 70% of the total current flows through the dense pinch column [1], the average density for this value of 2 MA during the first neutron pulse will be around $0.8 \times 10^{19} \text{ cm}^{-3}$.

After this period the plasma column is disturbed by instabilities (figure 7: 2(c), 3(a), (b)). Local disc-like plasma inrush into the magnetic field (figure 7: 3(a), 4(b) and (d)—on ‘plasma diode’ see paper 2) and strong luminescence of filament and copper vapour are seen (figure 7: 3(b), (c), 4(a), (d)). Later on (approximately by 50 ns) copper vapours near the anode centre disappear (figure 7: 4(b)), and the bright region of the picture starts to move to the upper part. At this stage the second pulses of HXR and neutron emissions (the 3rd and 4th pulses in the traces of figure 9 (a), (b)) start. In all our regimes they were higher compared with the first ones by 4 to 10 times.

Similar images were obtained as a result of the photographing of a plasma with the help of a pin-hole SXR camera with ns time resolution (figure 8—three-frame picture taken in a single discharge). Measurements of the height of the bright part of a plasma column gave us here approximately the same value as in the visible range. But its diameter—circa 1 cm—is larger than the filament in figure 7, and it coincides with the ‘halo’ around it.

In the absence of interferometric pictures of the pinch we attribute the brightest structure of the pinch to the current filamentation (i.e. with runaways—see above) whereas we consider the halo as the dense plasma part of it (thus the volume of the dense plasma column is 6.4 cm^3). The characteristic ‘confinement’ time Δt of the pinch lasts about 150 ns as seen from frame and streak pictures. This time interval coincides with the duration of the first HXR and neutron pulses (figure 9—the 1st and 3rd pulses on (a) and (b) traces). However in comparison with the ideal MHD growth time τ_i (the ratio of the pinch radius to the ion thermal velocity) this real time interval Δt is much longer. In fact measurements gave us $\Delta t = n \times \tau_i = nr/v_i = nr/(3kT/m_D)^{1/2}$ (where n is the coefficient, τ_i the inertial confinement time or ideal MHD growth time, r the pinch radius, v_i the ion thermal velocity, k the Boltzmann constant, T the plasma temperature and m_D the deuteron ion mass) with n changed within the limits 10–15 from shot to shot (compared with $\tau_i \sim r/v_{Ti} \sim 10^{-8}$ s).

This large pinch’s longevity can very likely be explained by a longitudinal component of the magnetic field generated during the implosion phase, considered in combination with the inverse pinch effect. Indeed the reason for the H_z -component is very simple. Namely, because a coefficient of

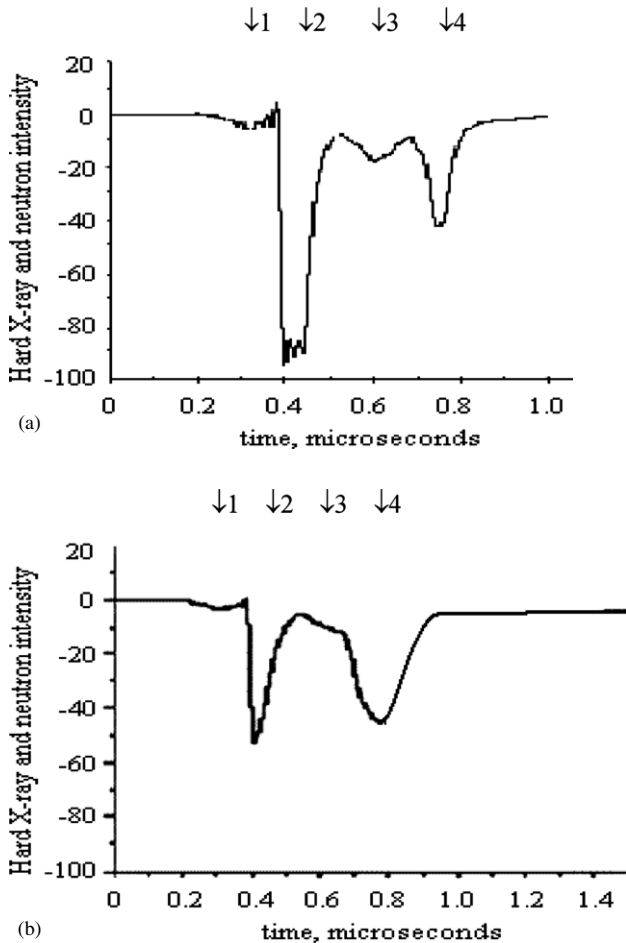


Figure 9. Hard x-ray (1st and 2nd pulses) and neutron signals (3rd and 4th pulses) taken in the same shot by SPD positioned at 0° , i.e. for neutron emission propagating along the direction of the Z-axis (head-on (a)) and at 90° to the Z-axis (side-on (b)) respectively.

symmetrical compression of PCS on its way to the Z-axis by ‘an effective radius’ (i.e. the ratio of the length from the upper part of the insulator to the final pinch radius) is equal to ~ 100 and the *surface* compression is about 10^4 . Any initial random magnetic field (Earth’s magnetic field, remnant magnetic fields from DPF constructions, initial magnetic field components of vortex structures of PCS at its formation, etc) will be captured by a highly conductive PCS and increased in this degree namely. The presence of this field (of magnitude $|\mathbf{H}_z| \sim 0.1|\mathbf{H}_\phi|$, a comparable value with the external azimuthal one) was experimentally ascertained in two independent experiments and by dissimilar techniques [9, 31]. This field has produced a stabilizing effect on the pinch [32]. Another possible mechanism of pinch stabilization has a dynamic nature. It is a plasma flow along the axis (a cumulative stream, which produces a shock wave above the pinch). When the deuterium shots were fired in the Z machine at Sandia, calculations were performed which indicated that this is indeed the operable mechanism for the temporary stabilization [33]. If we take into account the length of the pinch (10 cm) and the maximum measured speed of this jet ($5 \times 10^7 \text{ cm s}^{-1}$) the time duration of this effect would be 200 ns, which is close to our figures. On the other hand, as was mentioned above, maximal plasma density (so-called ‘first compression’) is reached at the

moment following the current maximum by about $2 \mu\text{s}$, i.e. during the drop of the current pulse. It means stabilization by the inverse skin effect [34], i.e. by a force produced during the phase when current aimed to leave a skin-layer for the centre of the pinch must contribute to the confinement time. With this characteristic— Δt —we have a full collection of data on the pinch’s plasma—future hot dense ‘target’ to be bombarded by a fast ion beam.

After the investigation of the above described (let us say ‘usual’) regime we have examined other operational modes of the PF-1000 facility. As it was found, these regimes appear when the anode has the above described *mushroom-like cap* on its top. We have found two different types of plasma behaviour that take place for dissimilar cathode configurations of the DPF chamber, namely with short and long rods of the cathode. Current and current derivative oscilloscope traces look rather similar for both these regimes as well as in the previous ‘normal’ case. Yet many other discharge characteristics differ strongly for these two diverse cathode configurations.

In the first regime we had the cathode rods much longer compared with the anode length as shown in figure 2(a), (b). In this case the shock wave (SW) and the plasma-current sheath (CS) after travelling along the whole anode tube length (so-called ‘run-down phase’) can move easily in two directions—upwards along the cathode rods and radially towards the Z-axis upon the cap of the anode (implosion of the plasma shell). In contrast, in the second regime both anode and cathode electrodes have almost equal sizes (the geometry is shown in figure 2(c)). In the latter situation the external contact of the CS rests connected to the top of the cathode rods after the run-down phase during the whole time of the implosion of the sheath on the Z-axis thus implying certain restrictions on the plasma expansion in the Z direction.

In these experiments we have found using three- or four-frame visual-light cameras and SXR pin-hole cameras (both time-resolved and time-integrated) that the above-mentioned anodic hat-shaped obstacle (its radius is 1 cm larger than the anode radius) produces a bifurcation of the SW. Because of this the final pinch consists of two parts distinguished by their height (figure 10).

Namely, the SW at its collision with the cap’s protrusion (barrier) in the course of its turning around the anode edge was divided into two SWs. They become equal in height towards the end of their implosion (together with subsequent CSs). What is more, these two parts were compressed to the axis at *different* moments of time depending on the cathode geometry.

In fact, in the first case, when the cathode rods (figure 1(a)) are long, the part which is *closer* to the anode surface (to the line ‘anode’ in figure 11(a)), i.e. the ‘lower’ or left part of the pinch, is usually compressed *later* than the more distant (‘upper’ or right) part of the column. In contrast, in the second situation with the short cathode rods (figures 2(a),(c)) the *upper part* is *tardy* (as in figure 11(b)) compared with the lower one. It may also be seen in figure 10, where a sequence of 1 ns-exposure pictures for short cathode rods is presented. Figure 11(c) and (d) show time-integrated x-ray pictures for long and short cathode rods, respectively.

However in both situations the *highest compression of plasma* is reached in that ‘half-pinch’, which is compressed *earlier*. From figures 11(c), (d) it is clearly seen that the

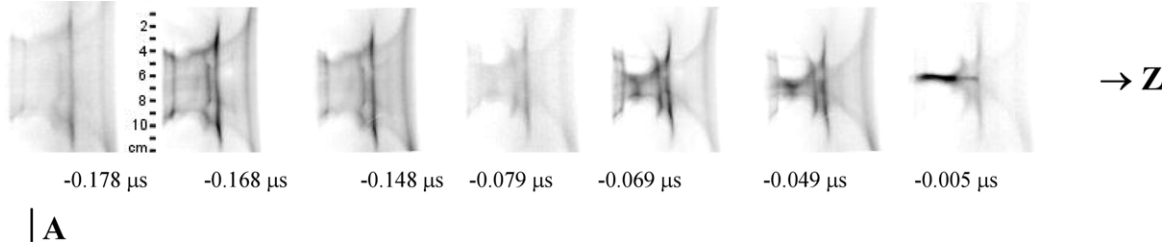


Figure 10. Time sequence of the SW bifurcation at the short cathode rods.

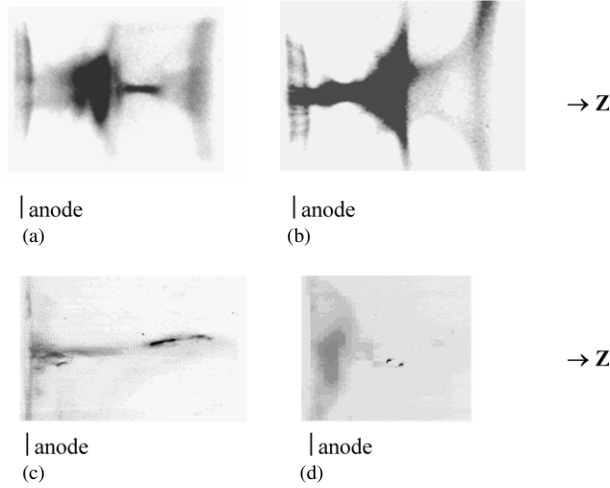


Figure 11. Visible ((a), (b), 1 ns time exposure) and soft x-ray ((c), (d), time-integrated) frame pictures for long ((a), (c)) and short ((b), (d)) cathode rods correspondingly.

brightest SXR luminosity relates to the ‘first compression’ (in figure 11(c) this is the upper part corresponding to the upper pinch of figure 11(a) and vice versa with figures 11(d), (b)). We have found that neutron yield is distinctly higher in the case of the long cathode rods when the highest mentioned plasma compression takes place at the ‘upper’ half-pinch and earlier.

This phenomenon of the SW decay can find its explanation on the basis of a simplified model based on an optical analogy, namely on the shock-wave diffraction at the abovementioned obstacle (in fact we have to discuss the diffraction of the dynamical SW + CS structure—‘plasma shell’). Indeed the diffracted wave must propagate at a certain angle ϑ to the primary wave:

$$\vartheta \cong \lambda/d, \quad (1)$$

where λ is the ‘wave-length’ of SW that can be estimated from figures 8 and 11 as a zone of the density (pressure) gradient at the front of SW and d is the characteristic size of the obstacle (protrusion) at the end of the cylindrical part of the anode (the push-through head of the cylinder). By substituting in the above equation $\lambda \cong 0.5$ cm and $d \cong 1$ cm we get an estimation for the height of the diffracted part of SW in the centre of the anode of radius $R \cong 10$ cm:

$$h \cong R \times \vartheta \cong R \times (\lambda/d) \cong 5 \text{ cm}. \quad (2)$$

This value coincides with the experimental one (approximately one half of the total pinch size). However the discussed reason for the bifurcation of SW at the obstacle

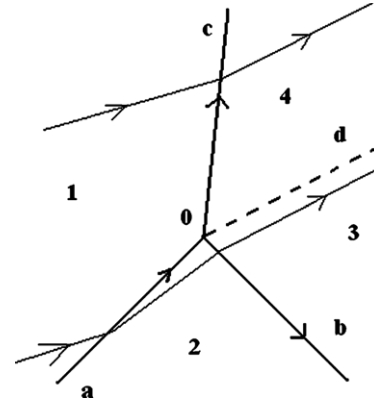


Figure 12. Scheme of the SW bifurcation.

does not explain the speed differences of the two pinches in the above two dissimilar cases. Its understanding can be found in a more refined examination of the phenomenon as follows.

As learned from many experiments and two-dimensional numerical simulations, the plasma shell (SW+CS) during its run-down phase travels as a slanting structure. The angle with respect to the generatrix of the anode cylinder is equal to about 45° and the shell is almost flat in the small. As is well known [35] a slanting shock wave in principle has the possibility to bifurcate into two upon an obstacle. Because, in our case, the diameter of the anode is much larger than the distance between our SW and CS, we may count this SW at each point of the obstacle’s circumference as a plane one (having as a matter of fact a cylindrical shape of a relatively large diameter). Then because the characteristic sizes of the pressure (density) gradient in front of the SW and the cap’s edge are much smaller than the characteristic size of the task (e.g. the diameter of the anode), we may neglect both these sizes and treat, in particular, the obstacle as a point-like one.

With these assumptions the problem can be examined as a two-dimensional one in each plane of the cross-section cutting the chamber through the Z -axis and with a *point of bifurcation* at the edge of the anode cap. In this case (see the scheme in figure 12) our slanting SW aO being initially a single one will decay into Ob and Oc .

It is easy to see that, side by side with these shock waves, the tangential discontinuity Od must exist which divides the two plasma streams propagating through Ob and Oc . As is shown in the literature [35] this line of discontinuity divides the flow into two regions (3 and 4), in which only two conditions must be fulfilled, namely the same *velocity directions*:

$$v_3 \parallel v_4 \quad (3)$$

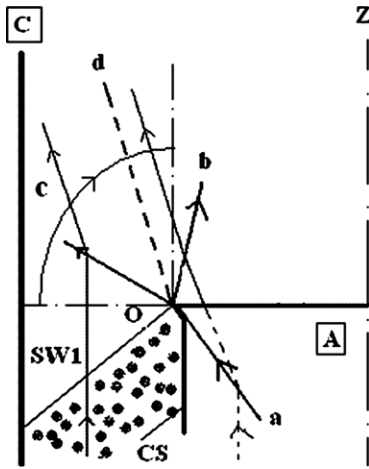


Figure 13. Real bifurcation of SW1 (*a*) in DPF on the obstacle *O* with subsequent turning of the streams (SWs *c* and *b*) by 90° towards the *Z*-axis following the circular arrow.

and the same pressure:

$$\rho_3 v_3^2 = \rho_4 v_4^2, \quad (4)$$

where v_3 , v_4 and ρ_3 , ρ_4 are velocities and densities in plasma streams of regions 3 and 4.

It means that in both regions (3 and 4 in the scheme of figure 12 or in the upper and lower pinches of figures 10 and 11) we shall have the same directions of SW + CS propagation. But in the case of long cathode rods when CS can freely expand in the *Z* direction the density inside the upper part of the pinch (or in the region 4) ρ_4 becomes lower thus increasing the velocity v_4 according to the relationship (4). In contrast, in the case of short cathode rods the upper part of the plasma stream (SW + CS) is compressed relatively to a higher degree because CS is now locked to the cathode end and restricted in its movement in the *Z* direction. That is why in this case the lower pinch (or the region 3) now has lower density ρ_3 and higher velocity v_3 .

In our real DPF situation the scheme of figure 12 should be modified taking into consideration the fact that after a so-called ‘run-down’ phase of SW + CS acceleration between anode (A) and cathode (C) in a direction *parallel to Z*, our magnetic field of current turns the plasma shell by 90° thus changing the above main acceleration direction into a *radial collapse to the Z*-axis. Thus the above picture in the DPF configuration will look as shown in figure 13 where one has to turn the upper part of the flow by 90° around point *O* along the circular arrow.

In connection with the above presented model we have to make four remarks. The first one is connected with the fact that because we deal with the collision of a relatively strong SW in plasma with a solid surface, a more accurate examination of the problem has to taken into account as well as a boundary layer and thermo-conductivity.

Secondly, generally speaking there is a principal difference between a front of a linear wave (as at diffraction of light or acoustic waves) and an SW front. Namely, SW velocity at a given point depends on its intensity, thus the geometry of a task is determined additionally by the particular SW intensity (e.g. SW angle of reflection is not simply equal to the angle of incidence). The third point is related to the fact that in our

case the whole process is ruled by a current flowing along CS (namely, its magnetic field pressure is the piston producing SW), thus the problem is related to *magnetohydrodynamics*. Moreover, as is stated in monographs on these issues (see e.g. [36]), the problem of interaction of a strong slanting shock wave with a solid barrier can be described at the present time only by a simplified theory, whereas a rigorous analytical one is absent. The majority of non-trivial cases here are investigated experimentally.

Thus the above remarks mean that the following steps in understanding the phenomenon can be reached by a more detailed *experimental* examination of the observed event done in a close vicinity of the obstacle and by a numerical simulation of the problem.

The fourth note is connected with the well-known fact that usually any *line* (or *surface*) of tangential discontinuity diffuses sooner or later into a turbulent layer. In our case it has an important consequence. Indeed the *current disruption phenomenon*, which is intrinsic to a DPF (see paper 2), can usually take place randomly in *various* cross-sections of the pinch column. In contrast, it finds in this situation its particular predominant place: namely near the border between the two pinches and usually in the lower part of the column (see figures 14(a),(b)).

Interesting results in the described regime with short cathode rods have been achieved when increasing the initial pressure of the working gas. In this case the velocity of the lower part of SW + CS has been decreased and it becomes equal to the upper one. The resulting dynamics of plasma may be seen in the three-frame sequence of figure 15. One may see that in this case on the border between the abovementioned two (‘upper’ and ‘lower’ or left and right in this picture) pinches a plasma blob is created, which has a long lifetime: $\Delta t \geq 10\tau_i$, where $\tau_i = R_p/v_i$ with R_p the pinch radius and v_i the ion thermal velocity.

It is evident that this relatively long confinement of the plasma formation is ruled by a naturally formed cusp-like magnetic field configuration, produced by Rayleigh–Taylor instability, which is developed on both pinches simultaneously.

In comparison with the previous cases the confinement time Δt is increased by a factor of circa 2.5. It is also reflected in neutron emission: the second neutron pulse for *optimal* initial gas pressure of figure 14(c) (firm line) has a duration of approximately 175 ns (FWHM), whereas the same neutron pulse for *high* initial pressure, see figure 14(c) (dashed line), lasts 450 ns when measured on the FWHM level (both curves are normalized in arbitrary units here). However, the volume of the plasma blob V_b having characteristic size circa 2.5 cm is $V_b = 4/3(\pi R^3) \leq 10 \text{ cm}^3$, i.e. about 3–4 times smaller compared with the pinch volume in the first regime of the PF-1000 operation (25 cm^3). So it is not surprising that the absolute neutron yield in this very case has not increased (in fact it was about the same as in the case shown in figures 6–10) compared with the previous regimes, as might be expected, because of the plasma confinement time increase. Additional analysis has also shown that a too high initial gas pressure reduces plasma shell velocity, and as a whole that results in time mismatching of its arrival at the *Z*-axis in relation to the current maximum. Because of this fact the moment of neutron production shifts to a later time when we have, accordingly, *lower absolute value of current*.

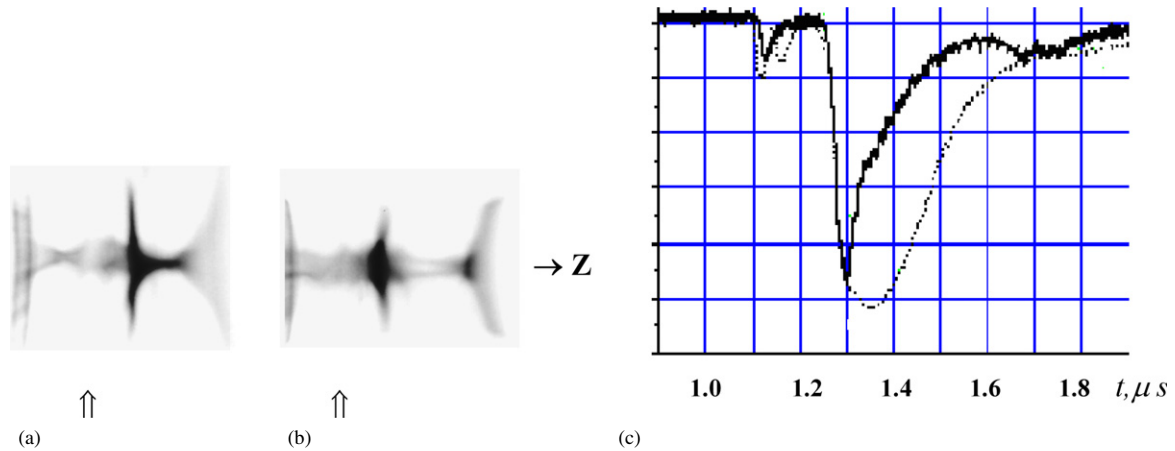


Figure 14. Frame pictures of the final implosion stage of a pinch in the case of optimal (a) and higher (b) initial gas density with arrows showing plasma column disruption (gap), shown in relation to corresponding temporal evolution of neutron emission (arbitrary units) (c) at the double-pinch (firm line) and cusp-like plasma (dashed-line curve) structures (the vertical scale of the neutron pulse for the cusp is increased by about three times for demonstrational purposes).

(This figure is in colour only in the electronic version)

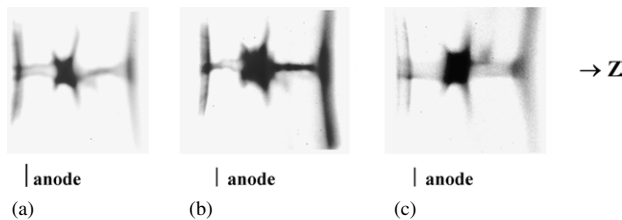


Figure 15. Three-frame picture of pinch dynamics taken in one shot for the conditions of short cathode rods and high initial pressure (time interval between frames—20 ns).

On the whole the described phenomenon of SW + CS bifurcation might give an optimistic opportunity for the future of large DPF devices. Indeed, as mentioned at the beginning of the paper, the expected thermal load on the central part of the DPF anode in these big devices operating with a high repetition rate may be of the order of 1 MW cm^{-2} . We shall have sputtering of the material here in any case. In fact, even at the proper cooling of the anode by e.g. water, it will be vaporized because of the powerful relativistic electron beam, which self-focuses along the Z -axis and strikes the central part of the anode. To prevent its damage the only foreseen way is to create here a *plasma layer* (so-called ‘inertial electrode’—(IE)) instead of the anode cap (or at least its central part).

For example, this plasma IE can be produced by an independent SW formation *inside* the anode tube, which will be pushed from the bottom to the upper part of it (see figure 2(a)) to substitute for the anode lid (the cap of the cylinder) at a proper moment in time. Namely its arrival at the anode upper section should be synchronized with the DPF pinch formation at the anode centre. In this case this complementary SW plasma will accomplish electrical contact with the anode tube along a circumference of large diameter. The electron beams will go inside the anode tube through this plasma layer and spread over a much larger surface of it.

However our present experiment has shown that instead of producing this ‘plasma anode’ by external means, we may use the above described phenomena of the SW bifurcation upon

upper anode widening. It can help us to produce automatically the ‘*inertial plasma electrode*’ during the discharge at the *proper place and time*. It seems quite clear that this plasma ‘inertial electrode’, which appeared in these experiments, may resolve a foreseeable risk of future difficulties with the high repetition rate DPF, but in particular with their next generation (above 10 MJ). Indeed the most loaded part of such a device—centre of the anode—may be changed routinely by plasma of such a kind. This plasma sheath has to have a much larger circumference of contact with the anode, which can now be done with a big hole in its centre. Consequently, the heat energy would spread over a much larger surface of metal, from which it can be removed much more easily by water cooling.

We shall discuss the radiation characteristics of PF-1000 in the second paper. But at the present time, according to the results described, it is seen that at the available configuration of the PF-1000 facility the parameters of the ‘target’ constitute the main feature influencing the neutron emission. We can control the neutron emission of the PF-1000 facility by changing these characteristics. Indeed with the present geometrical configuration we may change only the charging voltage and filling gas pressure. Within a small range of their optimal values we cannot change formidably the total current and consequently the parameters of the beam. But by these U_0 and p_0 changes, as well as by the anode geometry, we can control the final pinch plasma parameters.

As for the electrode shape changes, there are several promising possibilities to be checked in future. The simplest one is to make the central electrode shorter. In this case PCS will arrive much earlier at the Z -axis provided that the same initial pressure p_0 is used. Thus it may give a possibility to further increase the initial gas pressure provided that the proper surface breakdown conditions will be preserved on the insulator. In turn it gives the possibility to match electrical circuit parameters with the PCS dynamics and to reach a higher final plasma density of the pinch. Another opportunity is connected with the anode shape. It is known that spherical electrodes give better pinch parameters than rectangular ones [37]. In this case contrarily to the

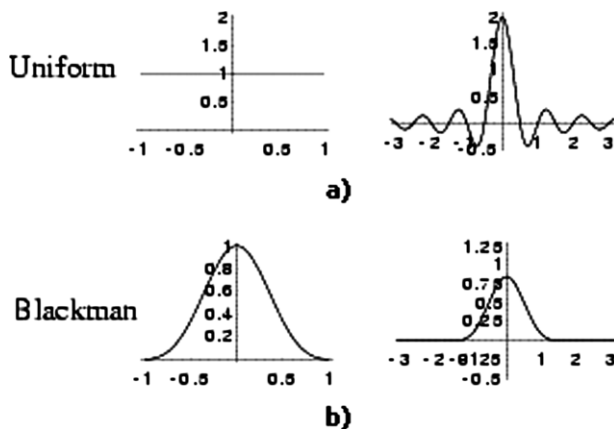


Figure 16. Instrument functions (right) with dependence on uniform (upper left) and apodized (bottom left) input functions.

cylindrical (rectangular in its cross-section) Mather's geometry the magnetohydrodynamic flow of PCS proceeds smoothly and results in higher plasma compression. But there is probably an even better opportunity.

Figure 16 presents two results of the interaction of *electromagnetic* waves with an obstacle—uniform input function and apodized one versus their resulting instrument functions (see e.g. [38]). It is clearly seen how the apodization procedure can suppress all diffraction oscillations at the edges. Such an effect can be produced either by an obstacle with a tailored wave penetration or by a special shape of an obstacle. It has to be mentioned however that in some cases for our goals just the *opposite* procedure producing cumulation of the plasma on the *Z*-axis (of the type of compression force profiling as in the super-compression of pellets in laser fusion) could be useful.

Another interesting opportunity might be provided by the above described double-pinch and cusp formations in the case when DPF operated with noble gases filling its chamber (e.g. with neon). In this case it is possible to reach an efficiency of soft x-ray generation of circa 10% with the radiation being almost monochromatic (concentrated mainly in a resonance line of H-like neon ~ 1 keV) and having a pulse duration of a few ns. Repetition rate of the device can be of about 10 cps [17]. It is interesting to check whether such a scheme could be used for a hohlraum target irradiation scheme as is discussed for wire arrays [39, 40]. The evident twofold benefits of a DPF over the wires might be *automatic* formation of two pinches one above the other as proposed in [39] and a high repetition rate with about the same soft x-ray production efficiency.

It is a well-known fact that the main neutron yield is always generated during the *second* pulse at each shot, i.e. in the pulse which appears *after* the phenomenon of the current abruption. Our PF-1000 device is not excluded from this rule.

This last event takes place somewhere in the middle of the plasma column, in particular, near the border between the two above described pinches when we have an anode obstacle for PCS. Ions produced here have a predominant drift directed to the cathode side of the chamber, i.e. to the upper part of the pinch. We have seen that in the regimes with two pinches the highest compression (i.e. the highest density of the hot plasma target) is produced within the pinch, which is

compressed *earlier*. That is why it seems unsurprising that in the case of the long cathode rods (i.e. when the highest density is reached in the pinch produced further from the anode as in figures 11(a) and (c)) we have obtained the highest neutron yield. It should be remarked here that the neutron pulse duration in these experiments coincides with the plasma 'target' confinement time.

5. Conclusions

The results of the experimental study presented in this paper gave the main parameters of dense plasma column—dense pinch, which is produced in the PF-1000 facility at its upper energy limit and with its present-day configuration. The column of dense plasma at the moment of its maximal pinching has a diameter of about 1 cm with a height of about 10 cm. Temperature estimations related to this 'first compression' stage give us values in the range 1.2–1.4 keV. Plasma density evaluation results in figures within the limits of $0.7\text{--}0.9 \times 10^{19} \text{ cm}^3$. Confinement time of the pinch is about 150 ns in usual regimes, which is several times larger than the ideal MHD growth times of plasma. These data constitute the initial characteristics of the future 'target' parameters to be 'exploited' in a subsequent self-irradiation of the pinch by an ion beam generated during the last phase of the kinetic stage of the DPF processes evolution.

These data give evidence also for the possibility of controlling plasma pinch parameters (such as its confinement time, plasma dynamics, etc) by several methods—not only by changes of initial gas pressure and battery charging voltage, but by geometry of the electrodes as well. This last can formidably change pinch configuration.

The PF-1000 device characteristics, which can be changed (and improved) in the frame of the present (unchanged) chamber configuration, are the *pinch plasma characteristics* (i.e. 'hot target' ones—not ion beams). It also opens perspectives for construction of future high-power devices by use of the so-called 'inertial electrode'. When it starts operating with noble gases it might be used probably in a hohlraum scheme of irradiation of a solid target, i.e. applied for inertial confinement fusion systems. Hopefully these facilities will be used in the nearest future as a powerful neutron source for radiation material science.

However, based on the results of this and following papers, further improvement of the PF-1000 facility becomes clear. First of all we need to change its geometry, which will be discussed in detail in paper 2. In particular it is obvious that the length of the device's anode has to be cut down. Then the circuit/chamber matching conditions will immediately demand a further increase in the initial pressure of working gas that, in turn, might improve the final 'target' characteristics together with the neutron production efficiency. But as will be seen from the second paper, a geometry change, both of the chamber and of the collector, might also result in beam characteristics improvement.

Physical data obtained in the course of these experiments, which are connected with the diffraction/bifurcation/reflection of SW upon the obstacle at the anode edge, also result in the specific important conclusion: the best configuration of a DPF anode might not be a cylinder. It has to be found along the

way taking into consideration these bifurcation phenomena, e.g. with the *apodized* shape of the anode as it is used in optics to eliminate diffraction pattern or *vice versa* to use special measures to stress SW + CS *diffraction effects*.

Acknowledgments

The work was supported in part by the International Atomic Energy Agency grant Nos 11940, 11941 and 11942 and by the Federal Agency on Atomic Energy of Russian Federation.

References

- [1] Bernard A *et al* 1998 *J. Moscow Phys. Soc.* **8** 1–93
- [2] Borisov V M and Khristoforov O B 2000 *Encyclopedia of Low Temperature Plasma* ed V E Fortov vol 2 (Moscow: Nauka) pp 350–7 (in Russian)
- [3] Pejovic M M, Ristic G S and Karamarkovic J P 2002 *J. Phys. D: Appl. Phys.* **35** R91–R103
- [4] Filippov N V *et al* 1971 *Plasma Physics and Controlled Nuclear Fusion Research (Madison, USA)* IAEA CN-28/D-6
- [5] Gribkov V A *et al* 1990 *Proc. IV Latin-American Workshop on Plasma Physics (Buenos Aires, Argentina)* p 120
- [6] Gribkov V A, Krokhnin O N, Sklizkov G V, Filippov N V and Filippova T I 1976 *Proc. P N Lebedev Physical Institute* vol 85 (New York: Allerton) pp 193–221
- [7] Gribkov V A 1976 *Energy Storage, Compression, and Switching* ed W Bostik *et al* (New York: Plenum) pp 271–8
- [8] Gribkov V A *et al* 2000 Pinch methods of plasma generation *Encyclopedia of Low Temperature Plasma* ed V E Fortov vol 2 (Moscow: Nauka) pp 358 (in Russian)
- [9] Gribkov V A *et al* 1980 Neutron-physics researches *Proc. P N Lebedev Physical Institute* vol 127 (New York: Allerton) pp 32–61
- [10] Gribkov V A 1993 *Chin. Phys. Lett. Suppl.* **10** 26–36
- [11] Petrov D I, Filippov N V, Filippova T I and Khrabrov V A 1958 *Plasma Physics and Controlled Fusion Research* vol 4 (Moscow: Academy of Sciences of the USSR) pp 170–81 (in Russian)
- [12] Mather J M 1965 *Phys. Fluids* **8** 366–77
- [13] Gribkov V A, Denus S, Dubrovsky A V, Kalachev N V, Krokhnin O N, Sledzinski S and Chekai S 1987 *P N Lebedev Physical Institute Reports* No 3, pp 28–30
- [14] Krompholz H, Michel L, Schonbach K H and Fischer H 1977 *Appl. Phys.* **13** 29
Jäger U and Herold H 1987 *Nucl. Fusion* **27** 407
- [15] Volobuev I V, Gribkov V A, Denus S and Krokhnin O N 1987 *P N Lebedev Physical Institute Reports* No 11, pp 32–4
- [16] Bogolyubov E P *et al* 1998 *Phys. Scr.* **57** 488
- [17] Lee S, Lee P, Zhang G, Feng X, Gribkov V A, Liu M, Serban A and Wong T K S 1998 *IEEE Trans. Plasma Sci.* **26** 1119
- [18] Tartari A *et al* 2004 *Nucl. Instrum. Methods Phys. Res. B* **213** 607
Scholz M, Bienkowska B and Gribkov V A 2002 *Czech. J. Phys. (Suppl.) D* **52** D85
- [19] Sadiq M, Shafiq M, Waheed A, Ahmad R and Zakauallah M 2006 *Phys. Lett. A* **352** 150
- [20] Rawat R S, Chew W M, Lee P, White T and Lee S 2003 *Surf. Coat. Technol.* **138** 159
- [21] Gribkov V A 1993 *J. Moscow Phys. Soc.* **3** 231
- [22] Herold H, Jerzykiewicz A, Sadowski M and Schmidt H 1989 *Nucl. Fusion* **29** 1255
- [23] <http://www.frascati.enea.it/lfmif/>
- [24] Gribkov V A *et al* 2003 *J. Phys. D: Appl. Phys.* **36** 1817–25
- [25] Scholz M, Miklaszewski R, Gribkov V A and Mezzetti F 2000 *Nucleonika* **45** 23
- [26] Gribkov V A, Karpinski L, Strzyzewski P, Scholz M and Dubrovsky A V 2004 *Czech. J. Phys. (Suppl.) C* **54** C191–7
- [27] Rager J P 1981 *Preprint CNEN-81.19/cc* Centro di Frascati, Rome, Italy
- [28] Herold H, Kaeppler H J, Schmidt H and Shakhatre M 1988 *Z-pinch and Plasma Focus Workshop (Nice)* (Paris: Ecole Polytechnique) pp 44–55
- [29] Scholz M, Miklaszewski R, Paduch M, Sadowski M J, Szydłowski A and Tomaszewski K 2002 *IEEE Trans. Plasma Sci.* **30** 476
- [30] Schmidt H, Kasperczuk A, Paduch M, Pisarczyk T, Scholz M, Tomaszewski K and Szydłowski A 2002 *Phys. Scr.* **66** 168
- [31] Ehrhardt J, Fischfeld G, Kirchesch P, Hubner K and Rager J P 1981 Experimental evidence for B_z -field and microturbulences in the Frascati PF facility *10th European Conf. on Controlled Fusion and Plasma Physics (Moscow)* Post-deadline paper
- [32] Bittencourt J A 1988 *Fundamentals of Plasma Physics* (Oxford: Pergamon) pp 357–60
- [33] <http://zpinch.sandia.gov/>
- [34] Libin Z 1927 *J. Prikladnoj Fiz. (J. Appl. Phys.)* **IV** 45 (in Russian)
Culverwell I D, Coppins M, Haines M G, Bell A R and Rickard G J 1989 *Plasma Phys. Contr. Fusion* **31** 387
- [35] Landau L D and Lifshitz E M 1988 *Gidrodinamika (Hydrodynamics) Theoretical Physics* 4th edn (Moscow: Nauka) vol VI, p 581 (in Russian)
- [36] Witham G B 1974 *Linear and Nonlinear Waves*, (New York: Wiley)
- [37] Sarov 1996 *Physics and Technology of Pulsed Sources of Ionizing Radiations for Investigations of Fast Transient Processes* ed N G Makeev (Sarov: VNIIF) (in Russian)
- [38] <http://mathworld.wolfram.com/ApodizationFunction.htm>
- [39] Matzen M K *et al* 2005 *Phys. Plasmas* **12** 055503
- [40] Alexandrov V V *et al* 2001 *Plasma Phys. Rep.* **27** 89
Sasorov P 2006 Dynamics of plasma jets in multiwire arrays *DENSE Z-PINCHES: 6th Int. Conf. on Dense Z-Pinches (Oxford, UK 25–28 July 2005)* ed J Chittenden *AIP Conf. Proc.* **808** 81–4